

# Yang–Mills topology on four-dimensional triangulations

Giuseppe Clemente,<sup>1,\*</sup> Massimo D’Elia,<sup>1,†</sup> Dániel Németh,<sup>2,3,‡</sup> and Gianmarco Simonetti<sup>1,§</sup>

<sup>1</sup>*Dipartimento di Fisica dell’Università di Pisa and INFN — Sezione di Pisa, Largo Pontecorvo 3, I-56127 Pisa, Italy.*

<sup>2</sup>*Institute for Mathematics, Astrophysics and Particle Physics,*

*Radboud University, Heyendaalseweg 135, 6525 AJ Nijmegen, The Netherlands*

<sup>3</sup>*Institute of Theoretical Physics, Jagiellonian University, Łojasiewicza 11, Kraków, PL 30-348, Poland.*

We consider 4D  $SU(N)$  gauge theories coupled to gravity in the Causal Dynamical Triangulations (CDT) approach, focusing on the topological classification of the gauge path-integral over fixed triangulations. We discretize the topological charge and, after checking the emergence of topology and the continuum scaling on flat triangulations, we show that topology emerges on thermalized triangulations only in the so-called  $C$ -phase of CDT, thus enforcing the link between such phase and semi-classical space-time. We also provide a tool to visualize the topological structures.

*Introduction* — Triangulations are useful lattice discretizations of curved space-times [1], which are represented as the gluing of elementary pieces of flat space-times known as simplices, like triangles in 2D, tetrahedra in 3D, and so on. They are also the basis for the approach to Quantum Gravity (QG) known as Dynamical Triangulations (DT), consisting in the representation of the Euclidean QG path-integral in terms of such configurations, where one looks for the presence of a critical surface within the space of bare parameters as a possible location for a physical, renormalized theory. A particular version of this program, in which causality is enforced by requiring a well-defined time foliation of the triangulation (Causal Dynamical Triangulations or CDT [2, 3]) is revealing particularly promising in 4D space-time, because of the presence of a non-trivial phase diagram with critical surfaces at the boundary of regions where semi-classical features emerge.

Within this context, the study of quantum field theories (QFT) coupled to triangulations is of utmost importance. First, it provides an effective tool for a numerical study of QFT on curved space-time, which is interesting by itself. Secondly, the path towards renormalized QG should go, sooner or later, through a full formulation of the theory coupled to other fields of the standard model. In this respect, gauge field theories are a primary goal.

While the program of coupling gauge fields to CDT has been fully accomplished in the 2D case [4–6], its extension to 4D seems more difficult, at least when trying to build a Markov Chain capable of easily exploring the configuration space of the full theory [7]. From this point of view, the present study should be considered as an intermediate step, yet addressing an important aspect.

We will consider the formulation and simulation of  $SU(N)$  gauge theories discretized on quenched triangulations, meaning that the space-time geometry will stay fixed while gauge fields evolve, although we will repeat the study for different triangulations, going from quasi-flat to those taken from the standard CDT path-integral. Among the different possible gauge invariant observables, we will focus on the definition of gauge topology.

There are at least two good reasons for that. First, the

classification of the path-integral of 4D  $SU(N)$  gauge theories into topological sectors is at the basis of many non-perturbative features of such theories, including Quantum ChromoDynamics (QCD), like the non-trivial dependence on the CP violating parameter  $\theta$ . Second, such topological classification is intimately connected to the structure of space-time itself, since it measures the winding of gauge fields on the space-time boundary over the gauge group. For instance, it seems hard to find non-trivial topology on triangulations with effective dimension less than four (e.g., the branched polymer or collapsed phases of the DT theories), similarly to what happens for QCD at asymptotically high temperatures, which is effectively three-dimensional and for which indeed topological fluctuations are strongly suppressed.

Therefore, the study of gauge field topology may help to better characterize the properties of the space-time configurations sampled in CDT simulations, in a novel way that has never been considered before. From a merely algorithmic point of view, the very definition of topology will require to fix a global orientation for the triangulation, a problem which has not been afforded in previous studies and will be treated in the following.

*Implementation* — Our program goes through three main steps: discretization of gauge fields on a given triangulation, assignment of a probabilistic weight reproducing the Yang–Mills path integral in the continuum and numerical sampling of it, definition and numerical study of an observable reproducing topology in the continuum.

As for the first step, it is natural to assign a different local gauge choice to each simplex; this is also the only (apart from  $d = 2$ ) way to get the correct counting of degrees of freedom. In this way, the elementary gauge variables are the  $SU(N)$  parallel transporters connecting pairs of adjacent simplices, i.e. associated to links of the dual graph [6, 7]. The most elementary Yang–Mills action on a fixed triangulation  $\mathcal{T}$  is then written in terms of the *plaquette*  $\Pi_b$ , i.e., the product of dual link variables around the  $(d-2)$ -simplex  $b$  (a triangle in 4 dimensions), where  $n_b$  is the number of  $d$ -simplices around  $b$ . The area enclosed by an elementary plaquette is  $\mathcal{A}n_b$ , where  $\mathcal{A}$  is an elementary area (e.g.,  $1/3$  of the simplex area in 2D),

so that the correspondence with continuum field strength reads:

$$\Pi_b \simeq \exp(ig n_b \mathcal{A} F_{\mu\nu}) \quad (1)$$

where  $\mu\nu$  is a pair of directions orthogonal to  $b$  and  $g$  is the bare coupling constant. The second order expansion of  $\text{Tr}(\Pi_b)$  gives, apart from constant additive factors,  $-N n_b^2 g^2 \mathcal{A}^2 \text{Tr}(F_{\mu\nu}^2)/2$ , so one can define

$$S_{\text{YM}} \equiv -\beta \sum_{b \in \mathcal{T}^{(d-2)}} \frac{\tilde{\Pi}_b}{n_b}, \quad (2)$$

where  $\tilde{\Pi}_b \equiv [\frac{1}{N} \text{ReTr}\Pi_b - 1]$ . The factor  $n_b \mathcal{A}^2$  counts the space-time volume pertaining to each  $b$ , apart from a missing factor  $\sqrt{5}$ , so the whole sum returns, in the naïve continuum limit, the volume integral of  $\text{Tr}(F_{\mu\nu}^2)$ , averaged over all possible directions, times a factor  $g^2/(2N\sqrt{5})$ ; the usual continuum expression of the Yang–Mills action coincides with this form, apart from a factor 6, coming from the sum over all orthogonal direction pairs. That finally fixes the relation between  $g$  and the inverse gauge coupling  $\beta$ :

$$\beta = \frac{12\sqrt{5}N}{g^2}. \quad (3)$$

The sampling of gauge configurations according to  $\exp(-S_{\text{YM}})$  can go through usual pure gauge algorithms, e.g., we adopted a standard heat-bath algorithm [8, 9]. Since only gauge variables are dynamical, the different space-time regularization keeps the asymptotic behavior of the lattice spacing  $a(\beta)$  unchanged up to two loops:

$$\bar{a} \equiv \Lambda_L a \simeq (\beta_0 g^2)^{\beta_1/(2\beta_0^2)} e^{-1/(2\beta_0 g^2)} \quad (4)$$

where  $3(4\pi)^2 \beta_0 = 11N$  and  $3(4\pi)^4 \beta_1 = 34N^2$  for pure Yang–Mills; of course both  $\Lambda_L$  and the regime where such asymptotic behavior sets in are a priori unknown.

As for the definition of topological charge, its continuum expression in 4D is the following:

$$Q = \frac{g^2}{32\pi^2} \int dx \varepsilon_{\mu\nu\alpha\beta} \text{Tr} [F^{\mu\nu}(x) F^{\alpha\beta}(x)]. \quad (5)$$

We can expand the expression for the strength tensor around the center of each simplex (i.e., a node of the dual graph) in terms of discretized variables in a local chart. Let us consider a specific simplex  $\sigma$  and an over-complete set of unit vectors  $\{\vec{e}_{A,\sigma}\}_{A=1,\dots,5}$ , directed from the center of  $\sigma$  to each of its 5 neighbors; these vectors are related to a flat Cartesian basis at  $\sigma$  via a change of basis, represented by the matrix  $e_{A,\sigma}^\mu$ . We can then write

$$F_{\sigma}^{\mu\nu} = e_{A,\sigma}^\mu e_{B,\sigma}^\nu \bar{F}_{\sigma}^{AB}, \quad (6)$$

where  $\bar{F}_{\sigma}^{AB}$  can now be related to the plaquette built by looping around the bone  $b_{(AB\sigma)}$  identified by the neighbors  $A$  and  $B$ :

$$\Pi_{b_{(AB\sigma)}} \simeq e^{ig \mathcal{A} n_{b_{(AB\sigma)}} \bar{F}_{\sigma}^{AB}} \simeq 1 + ig \mathcal{A} n_{b_{(AB\sigma)}} \bar{F}_{\sigma}^{AB}. \quad (7)$$

From Eq. (7) we can read off, at the leading order in  $a$

$$\bar{F}_{\sigma}^{AB} \simeq \frac{1}{g \mathcal{A} n_{b_{(AB\sigma)}}} \Im[\Pi_{b_{(AB\sigma)}}]; \quad \Im[\Pi] \equiv \frac{\Pi - \Pi^\dagger}{2i}. \quad (8)$$

Substituting into the expression for the topological charge density (Eq. (5) before integration), we obtain

$$\rho_{\sigma} \simeq \rho_{\sigma}^{ABMN} \bar{\varepsilon}_{ABMN,\sigma} \quad (9)$$

where we defined the charge four-form density as

$$\rho_{\sigma}^{ABMN} \equiv \frac{1}{32\pi^2 \mathcal{A}^2} \text{Tr} \left\{ \Im \left[ \frac{\Pi_{b_{(AB\sigma)}}}{n_{b_{(AB\sigma)}}} \right] \Im \left[ \frac{\Pi_{b_{(MN\sigma)}}}{n_{b_{(MN\sigma)}}} \right] \right\}, \quad (10)$$

and the Levi–Civita symbol as

$$\bar{\varepsilon}_{ABMN,\sigma} \equiv \varepsilon_{\mu\nu\alpha\beta} e_{A,\sigma}^\mu e_{B,\sigma}^\nu e_{M,\sigma}^\alpha e_{N,\sigma}^\beta \quad (11)$$

expressed in terms of a complete set of basis vectors. Finally, from Eq. (9) one can get the topological charge  $Q_L$  by integrating  $\rho_{\sigma}^{ABMN}$  over spacetime. This is achieved by multiplying the charge density by the volume  $V_{\sigma} = \sqrt{5}/96$  (in lattice units) of a simplex. An additional factor  $1/5$  stems from the five possible choices of the four independent directions used to build the components of the strength field tensor<sup>1</sup>. Explicitly,  $Q_L$  reads:

$$Q_L = \frac{1}{5} \sum_{\sigma \in \mathcal{T}} \rho_{\sigma} V_{\sigma}. \quad (12)$$

An essential point for correctly implementing this sum is that the vectors  $\vec{e}_{A,\sigma}$  in each simplex must be consistently ordered according to the global orientation of  $\mathcal{T}$ , which is well defined for the manifolds typically considered in CDT: that requires a careful algorithmic implementation, see Appendix A for more details.

Topology is well defined only in the continuum limit. A standard procedure, adopted on regular lattices to recover an approximate topological classification, is to iteratively smooth gauge configurations so as to remove ultraviolet noise, typically by minimizing the gauge action and exploiting the fact that topological sectors are characterized by local minima, corresponding to (anti-)instantons in the continuum. We will follow this

<sup>1</sup> Notice that this construction is very similar to the standard symmetrized clover discretization adopted on flat hypercubic lattices, where the number of links coming out from each site is 8, instead of 5 as in our case.

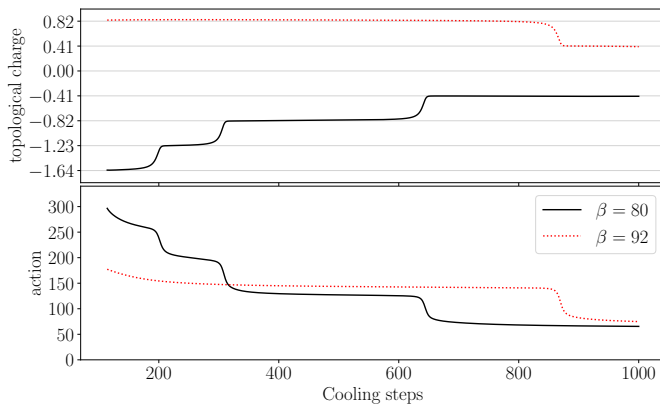


**FIG. 1:**  $Q_L$  and  $S_{YM}$  evolution during cooling for two  $SU(3)$  configurations sampled at different  $\beta$  values on quasi-flat triangulations with  $T = 40$ .

approach, exploiting in particular the so-called cooling algorithm [10–17].

*Numerical Results* — As a first, exploratory step, we consider quasi-flat configurations built from the triangulation of a hypercube with periodic boundary conditions [18, 19]: this is an important benchmark, since results should match those obtained on standard hypercubic lattices. We will illustrate results obtained for  $SU(3)$  with various numbers of time slices and  $\sim 10^3$  simplices per time slice; similar results have been obtained for  $SU(2)$ .

Fig. 1 shows the evolution of  $Q_L$  and  $S_{YM}$  during the action minimization for two sampled configurations: the appearance of long pieces of cooling histories where both quantities take almost constant values reveals, similarly to what observed in standard lattice studies, the presence of metastable configurations, candidate for being the discretized counterparts of continuum (anti)-instantons and characteristic of the separation of the path-integral into homotopy classes. Moreover, the metastable values reached by  $Q_L$  suggests that they are also multiple of a well defined charge unit, as expected.

This is clearer from the histograms of  $Q_L$ , shown in Fig. 2. After a sufficient number of cooling steps, the topological charge distribution gets peaked around integer multiples of an elementary unit  $Q_0$ , with  $Q_0 \simeq 0.41$  independently of  $\beta$ . In principle, one would expect  $Q_0 \simeq 1$ , however also on regular lattices discretization effects make  $Q_0 < 1$  even after smoothing: here such effects could be even larger, because of the approximate flatness of the triangulation. The assignment of each configuration to a topological sector is however well defined [20, 21]

$$Q = \text{round}\{Q_L/Q_0\} \quad (13)$$

where "round" denotes the approximation to the closest integer and  $Q_0$  is fixed by minimizing

$$\langle (Q_L/Q_0 - \text{round}\{Q_L/Q_0\})^2 \rangle. \quad (14)$$

The distribution of  $Q$  is wider at lower  $\beta$ , this is expected by the running of the lattice spacing with  $\beta$ . Indeed, the variance of  $Q$  is proportional to the topological susceptibility  $\chi \equiv \langle Q^2 \rangle / V$  where  $V = N_4 V_\sigma a^4$  is the 4D volume, proportional to the total number of simplices  $N_4$ ; therefore, being  $\chi$  a physical quantity,  $\langle Q^2 \rangle$  is expected to run as  $a^4$  at fixed triangulation. That gives us the possibility to check if the asymptotic continuum scaling of  $a$ , Eq. (4), is reached within the explored range of  $\beta$ .

To this purpose, we computed the dimensionless susceptibility  $\chi_{lat} \equiv \langle Q^2 \rangle / N_4$  for each data set. Since topological configurations are only metastable, the smoothing procedure, apart from cleaning the topological signal, leads also to a partial loss of it: for this reason, it is usual to perform an extrapolation to zero smoothing, choosing a suitable range of cooling steps for which unphysical fluctuations have already been killed while the unwanted loss of signal proceeds linearly with the smoothing: an example is shown in the upper side of Fig. 3.

The so-extrapolated quantity is shown in the lower part of the same Figure, where we report in particular  $\bar{a} \chi_{lat}^{-1/4}$  as a function of  $\beta$  for different values of the temporal extension  $T$ , where  $\bar{a}$  is the 2-loop  $\beta$ -function in Eq. (4). This combination should approach a constant value in the small coupling regime where Eq. (4) becomes a good approximation: our results show that, luckily enough, we have at least a small window where this is true. Moreover, the absence of  $T$ -dependence, within errors, shows that also finite size effects should be reasonably under control.

Assuming the standard pure gauge value from the Witten–Veneziano mechanism [22, 23],  $\chi^{1/4} \sim 180$  MeV, the measured value of  $\chi_{lat}$  gives us an estimate of  $a \simeq (\chi_{lat}/(\chi V_\sigma))^{1/4}$ . We get  $a \sim 0.2$  fm, or in terms of the dual lattice spacing  $a' = a/\sqrt{10} \sim 0.06$  fm, at the border of the explored region,  $\beta = 94$ . It is interesting to notice that this is in the same ballpark of lattice spacings where scaling sets in for standard lattices; moreover, that tells us a posteriori that the space-time extensions are at least  $O(1)$  fm for all explored values of  $\beta$ , which is consistent, at least for pure gauge theories, with the absence of significant finite size effects.

Let us now discuss the interesting case of thermalized configurations. Remarkably, out of the four phases appearing in 4D CDT [24, 25], we could observe the appearance of non-trivial  $SU(N)$  topological sectors only in the so-called de Sitter phase, representing semi-classical spacetimes [26] with emergent effective action consistent with the Hartle–Hawking (H–H) minisuperspace model [27], and even in this case only when the overall triangulation topology was that of a torus  $(S^1)^4$ , i.e. no plateaus were observed for  $S^1 \times S^3$ . In Fig. 4 we show some examples of the topological charge distribution: also in this case, after enough smoothing, a well defined peaked structure appears, with equally spaced peaks but

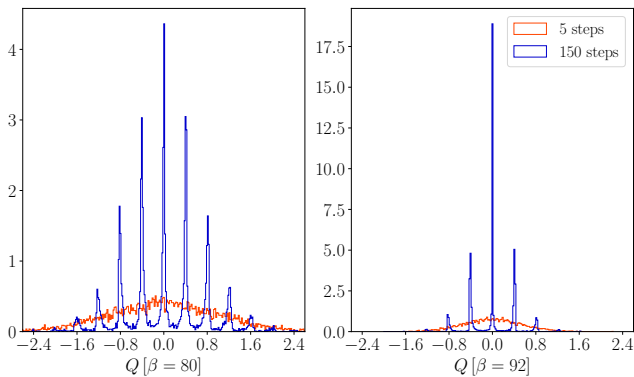


**FIG. 2:** Histograms of  $Q_L$  for  $SU(3)$  on quasi-flat  $T = 40$  triangulations after 5 (red) and 150 (blue) cooling steps.

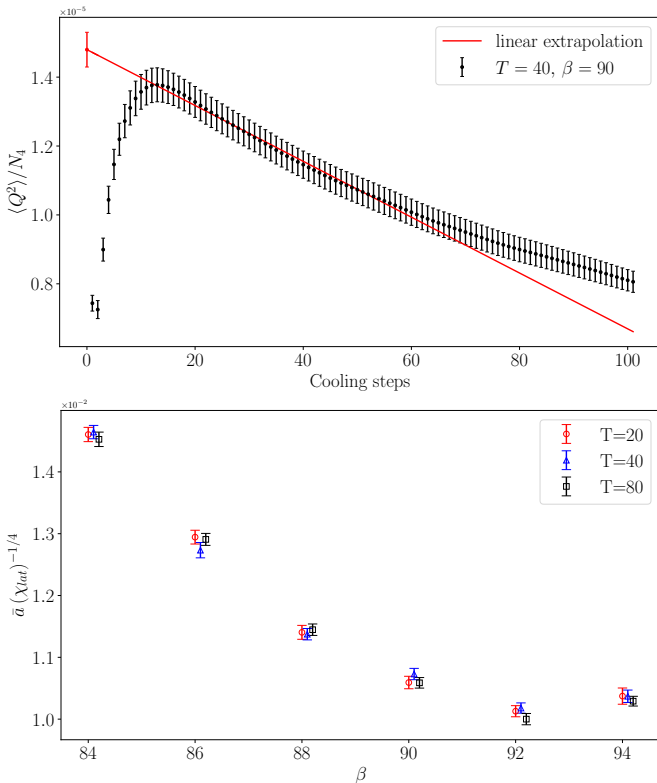


**FIG. 3:** Topological susceptibility for  $SU(3)$  gauge fields in a quasi-flat toroidal triangulation.

a spacing different from the quasi-flat, i.e.,  $Q_0 \sim 0.3$ .

We remark that, along the metastable plateaus, also  $S_{YM}$  is approximately a multiple of a well defined elementary unit  $S_1$ , which can be interpreted as the action contribution from a single (anti-)instanton. In the continuum, flat case one has [28]  $S_1 = 8\pi^2/g^2$  which, given our definition of  $\beta$  in Eq. (3), means  $NS_1/\beta = 2\pi^2/(3\sqrt{5}) \simeq 2.94$ . In Table I we show the estimates of  $NS_1/\beta$  obtained for  $N = 2, 3$  and for both quasi-flat and thermalized triangulations in the de Sitter phase. This quantity appears to be quite stable for different values

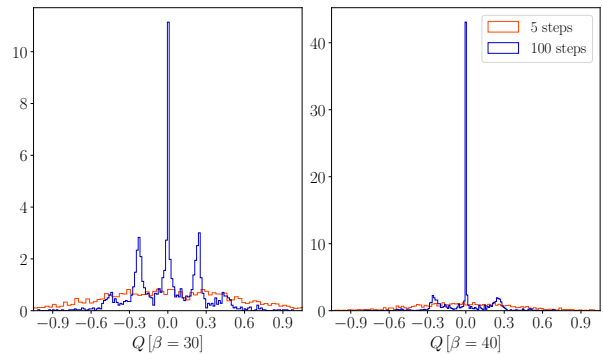


**FIG. 4:** Histograms of  $Q_L$  for  $SU(3)$  on triangulations thermalized in the de Sitter phase, with  $(S^1)^4$  overall topology, bare parameters  $\kappa_0 = 4.0, \Delta = 0, T = 20$  and  $N_4 = 120k$ .

of  $N$  and  $\beta$ , but it significantly varies depending on the ensemble of base manifolds. In particular, the quasi-flat estimate,  $NS_1/\beta \simeq 2.3(3)$  is not far from the flat semiclassical expectation 2.94, while a more significant renormalization appears for thermalized triangulations, where  $NS_1/\beta \simeq 1.1(2)$ .

*Visualization of non-trivial topological structures* —

In [29–31], a method was introduced to define pseudo-Cartesian coordinates in compact toroidal triangulated manifolds used in CDT (see the detailed discussion in Appendix B). By associating scalar field values  $\phi_x, \phi_y, \phi_z$  to each simplex (corresponding to  $x, y, z$ ) and using time foliation as  $t$ , a 4-coordinate system is formed. Cooling these scalar fields minimizes the scalar field action, effectively solving the inhomogeneous Laplace equation and approximating the classical solution. We used the extracted scalar-field values as a map and plotted the topological charge density within each simplex, with red for positive and blue for negative charges, as shown in Fig. 5 for the snapshot of a specific configuration, which is classified in the  $Q = 1$  topological sector, after 10 cooling steps. It is interesting to notice that, at this early stage of cooling, the topological charge is still substantially delocalized, i.e., many clusters appear: this is similar to

$N$	$\beta$	$NS_1/\beta$	
		quasi-flat	de Sitter phase
2	20	2.30(30)	1.10(20)
	24	2.28(25)	1.12(17)
	28	2.27(21)	1.09(18)
3	80	2.28(30)	1.07(23)
	86	2.28(28)	1.06(21)
	92	2.28(26)	1.08(20)

**TABLE I:** Observed values of the action gap between consecutive topological sectors. The value of  $NS_1/\beta$  expected in the continuum flat case, considering Eq. (3), is about 2.94.



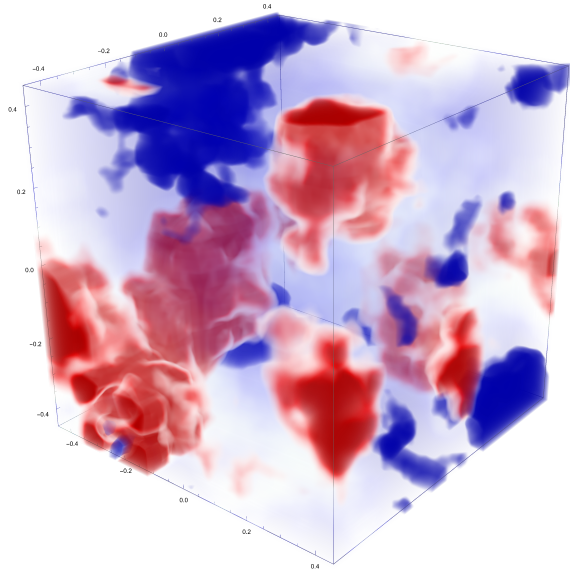


**FIG. 5:** A visualization of the charge density in  $\phi_x, \phi_y, \phi_z$  scalar-field coordinate representation after 10 cooling steps for  $\beta^{SU(2)} = 30$ , using the quasi-flat configuration. The topological charge density has been integrated in the time direction.

what is observed in standard lattice simulations; on the other hand, the same picture after prolonged cooling (which is not shown) appear as a single and well-defined cluster.

*Conclusions* — We successfully implemented  $SU(N)$  gauge fields on fixed triangulated manifolds, going from their numerical simulations to the definition and measurement of observables related to gauge topology. First, we verified the appearance of a topological classification of gauge configurations on quasi-flat triangulations, checking also the asymptotic scaling to the continuum limit of physical observables such as the topological susceptibility, and providing a framework to visualize the non-trivial topological structures. Then, we explored triangulations sampled from the CDT path-integral: remarkably, non-trivial gauge topology appears only in the de Sitter phase, thus enforcing the idea that such phase correctly reproduces semi-classical space-time, capable of sustaining non-trivial field-theoretic features such as gauge topology; the appearance of a non-trivial gauge topology seems also connected to the overall topology of the triangulation, an issue that should be further explored in the future. Future efforts should be devoted also to the definition of further gauge observables as well as, in a long term perspective, to the numerical simulation of the full gravity+gauge path integral.

*Acknowledgments* — GC and MD acknowledge support from Fondazione ICSC - National Centre on HPC,

Big Data and Quantum Computing - SPOKE 10 (Quantum Computing) and received funding from the European Union Next-GenerationEU - National Recovery and Resilience Plan (NRRP) – MISSION 4 COMPONENT 2, INVESTMENT N. 1.4 – CUP N. I53C22000690001. DN is supported by the VIDI programme with Project No. VI.Vidi.193.048, which is financed by the Dutch Research Council (NWO). The Numerical simulations have been performed at the IT Center of the University of Pisa, Jagiellonian University and Radboud University. DN thanks Jakub-Gizbert Studnicki and Andrzej Görlich for fruitful discussions and support with the code.

## APPENDIX A. REORDERING PROCEDURE

In order to have a meaningful implementation of the topological charge, the simplices of the triangulation must be properly oriented so that the pseudo-scalarity of  $Q$  holds. In the particular case of simplicial manifolds, this means that for any pair of adjacent simplices  $\sigma_{1,2} \in \mathcal{T}$ , the local frames  $\{\vec{e}_{\sigma_{1,2},A}\}$  already mentioned before, must coincide up to a roto-translation:

$$\vec{e}_{A,\sigma_2} = (R_{\sigma_2} \circ t_{\sigma_2 \leftarrow \sigma_1}) \vec{e}_{A,\sigma_1} \quad \forall A \in \{1, \dots, d\} \quad (15)$$

with  $R_{\sigma_2} \in SO(d)$  and  $t_{\sigma_2 \leftarrow \sigma_1}$  respectively a rotation defined in the center of  $\sigma_2$  and a translation which moves the center of  $\sigma_1$  to the center of  $\sigma_2$ . In other words, equation (15) just states that the two frames must have the same parity. In the following, we will show a possible strategy to fix a global orientation of  $\mathcal{T}$ . This method is simply based on setting the orientation of  $\{\vec{e}_{A,\sigma_2}\}$  assuming that  $\{\vec{e}_{A,\sigma_1}\}$  has already been fixed. To do so, we will make use of the vectors  $\{\vec{v}_{A,\sigma_{1,2}}\}_{A=1,\dots,d}$  which represent the set of vectors connecting the centers of  $\sigma_{1,2}$  to their vertices. Let us start first fixing  $\{\vec{v}_{A,\sigma_1}\}$ : this can be done for instance by symmetrizing and scaling<sup>2</sup>  $\{\vec{e}_{A,\sigma_1}\}$  with respect to the center of  $\sigma_1$ :

$$\vec{v}_{A,\sigma_1} = -\|\vec{v}\| \vec{e}_{A,\sigma_1} \quad \forall A \in \{1, \dots, d\}. \quad (16)$$

In this way, the two frames in the expression above have the same parity in even dimensions and opposite parity otherwise. At this point one just needs to fix  $\{\vec{v}_{A,\sigma_2}\}$  by requiring that the latter has the same orientation of  $\{\vec{v}_{A,\sigma_1}\}$  and use again (16) to retrieve  $\{\vec{e}_{A,\sigma_2}\}$  which eventually will satisfy (15). For this purpose, let us label with  $\{P_i\}_{i=1,\dots,d-1}$  the vertices of the  $d-1$ -dimensional subsimplex shared by  $\sigma_1, \sigma_2$ : if labels are chosen so that the association between such points and the first  $d-1$  vectors of  $\{\vec{v}_{A,\sigma_1}\}$  is

$$\{\vec{v}_{A,\sigma_1}\} = \{\vec{v}_{1,\sigma_1}(P_1), \dots, \vec{v}_{d-1,\sigma_1}(P_{d-1}), \vec{v}_{d,\sigma_1}\} \quad (17)$$

<sup>2</sup> We are assuming that  $\{\vec{e}_{A,\sigma}\}$  are unitary vectors.

then  $\{\vec{v}_{A,\sigma_2}\}$  can be obtained by exchanging two any directions after that the common vertices have been associated with the vectors of  $\sigma_2$  in the same way as for  $\sigma_1$ . Explicitly it reads

$$\{\vec{v}_{A,\sigma_2}\} = \tau_{jk} \{\vec{v}_{1,\sigma_2}(P_1), \dots, \vec{v}_{d-1,\sigma_2}(P_{d-1}), \vec{v}_{d,\sigma_2}\}, \quad (18)$$

where  $\tau_{jk}$  is a transpose operator acting as

$$\begin{aligned} \tau_{jk} \{\dots \vec{v}_{j,\sigma_2}(P_j), \dots, \vec{v}_{k,\sigma_2}(P_k), \dots\} \\ = \{\dots \vec{v}_{j,\sigma_2}(P_k), \dots, \vec{v}_{k,\sigma_2}(P_j), \dots\}. \end{aligned} \quad (19)$$

Indeed, since the uncommon vertices (one for each simplex) belong to each of the two separated space regions defined by the shared sub-simplex,  $\{\vec{v}_{A,\sigma_1}\}$  and  $\{\vec{v}_{A,\sigma_2}\}$  would have opposite parity if the action of a discrete operator like  $\tau$  was neglected. Such a procedure can be iterated for all the nearest neighbours of  $\sigma_1$  and therefore extended to all the simplices of the triangulation. Of course, this can be done consistently, up to pure rotations, only if the given triangulation is globally orientable.

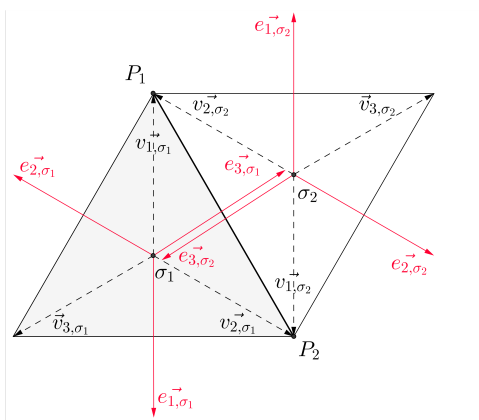


FIG. 6: Two-dimensional sketch of the ordering procedure.

## APPENDIX B. VISUALIZATION OF THE CHARGE DENSITIES

One way to add matter fields into a triangulated manifold is to treat the field as a map between the triangulated space-time  $\mathcal{M}_H(g_{\mu\nu})$  and a target space  $\mathcal{N}(h_{\alpha\beta})$  with fixed metric and topology. In case when the target space is Euclidean  $\mathbb{R}^d$  or  $S^d$  with a diagonal and flat metric on  $\mathcal{N}$ , then the continuum action

$$\begin{aligned} S_M[\phi, g] = \\ \frac{1}{2} \int d^4x \sqrt{g(x)} g^{\mu\nu}(x) h_{\rho\sigma}(\phi^\gamma(x)) \times \partial_\mu \phi^\rho(x) \partial_\nu \phi^\sigma(x) = \\ \frac{1}{2} \sum_{\sigma=1}^d \int d^4x \sqrt{g(x)} \partial^\nu \phi^\sigma(x) \partial_\nu \phi^\sigma(x) \end{aligned} \quad (20)$$

can be separated for each direction  $\sigma$ . The addition of a boundary allows the field values to technically obtain a winding number, but the added boundary-jump condition (with amplitude  $\delta$ ) renders the mapping to remain continuous by identifying

$$\phi_i^\sigma \equiv \phi_i^\sigma + n \cdot \delta, \quad n \in \mathbb{Z}, \quad (21)$$

at the boundary, mapping the field values to a circle with circumference  $\delta$ . The discrete form of the matter field action with this boundary term is

$$\begin{aligned} S_M^{CDT}[\phi, T] &= \frac{1}{2} \sum_{\sigma=1}^d \sum_{i \leftrightarrow j} (\phi_i^\sigma - \phi_j^\sigma - \delta \cdot \mathbf{B}_{ij}^\sigma)^2 = \\ &= \sum_{\sigma=1}^d \left( \sum_{i,j} \phi_i^\sigma \mathbf{L}_{ij}(T) \phi_j^\sigma - 2\delta \sum_i \phi_i^\sigma b_i^\sigma + \delta^2 \cdot V^\sigma \right) \end{aligned} \quad (22)$$

where  $\sum_{i \leftrightarrow j}$  counts all of the neighbors of the discrete building blocks and  $\mathbf{L}_{ij}(T)$  is defined as the discrete Laplace–Beltrami operator for the underlying dual graph. The boundary term  $\mathbf{B}_{ij}^\sigma$  gives a  $\pm\delta$  contribution if the particular simplex pair  $\{i, j\}$  lies on the boundary. Minimizing the above equation leads to

$$\mathbf{L}\phi^\sigma = \delta \cdot b^\sigma, \quad (23)$$

which is the inhomogeneous Laplace equation for the scalar field  $\phi^\sigma$  with a boundary term  $b^\sigma$  with scale  $\delta$ . Decomposing the scalar field as  $\phi^\sigma = \bar{\phi}^\sigma + \xi^\sigma$  and expanding the action leads to the form

$$\begin{aligned} S_M^{CDT}[\phi, \xi, T] &= \sum_{\sigma,i,j} \xi_i^\sigma \mathbf{L}_{ij}(T) \xi_j^\sigma + \\ &+ \sum_{\sigma=1}^d \left( \sum_{i,j} \bar{\phi}_i^\sigma \mathbf{L}_{ij}(T) \bar{\phi}_j^\sigma - 2\delta \sum_i \bar{\phi}_i^\sigma b_i^\sigma + \delta^2 \cdot V^\sigma \right) \\ &= \sum_{\sigma,i,j} \xi_i^\sigma \mathbf{L}_{ij}(T) \xi_j^\sigma + S_M^{CDT}[\bar{\phi}, T]. \end{aligned} \quad (24)$$

The classical solution  $\bar{\phi}^\sigma$  of the scalar fields obtains a winding number one and the quantum fields  $\xi^\sigma$  take real values with winding number zero.

We took thermalized pure gravity geometries with defined boundaries as a technical tool. For fixed geometries (in the quenched approximation) setting the value of  $\delta > 0$  and solving the inhomogeneous Laplace equation, Eq. (23), by cooling the dynamical scalar fields, we effectively forced the quantum fields  $\xi^\sigma$  to align with the classical solution  $\bar{\phi}^\sigma$ . Then extracting the scalar field coordinates for each simplex in directions  $(\phi_x, \phi_y, \phi_z)$  gave us a set of spatial coordinates and using the foliation  $t$  as a fourth coordinate and rescaling all coordinate values to one we obtain a  $[0, 1]^4$  box with a density inside that corresponding to the map from the underlying geometry to

the flat box. Associating to each simplex the topological charge density we can visualize it in this representation as the function of the scalar field coordinates, which is analogous to a Laplacian embedding of a graph. It was shown, that this map exhibits homogeneous large-scale properties only in the de Sitter phase.

---

\* [giuseppe.clemente@unipi.it](mailto:giuseppe.clemente@unipi.it)

† [massimo.delia@unipi.it](mailto:massimo.delia@unipi.it)

‡ [daniel.nemeth@ru.nl](mailto:daniel.nemeth@ru.nl)

§ [g.simonetti8@studenti.unipi.it](mailto:g.simonetti8@studenti.unipi.it)

- [1] T. Regge, *Nuovo Cim.* **19**, 558 (1961).
- [2] J. Ambjorn, A. Goerlich, J. Jurkiewicz, and R. Loll, *Phys. Rept.* **519**, 127 (2012), [arXiv:1203.3591](https://arxiv.org/abs/1203.3591) [hep-th].
- [3] R. Loll, *Class. Quant. Grav.* **37**, 013002 (2020), [arXiv:1905.08669](https://arxiv.org/abs/1905.08669) [hep-th].
- [4] J. Ambjorn, K. N. Anagnostopoulos, and J. Jurkiewicz, *JHEP* **08**, 016 (1999), [arXiv:hep-lat/9907027](https://arxiv.org/abs/hep-lat/9907027).
- [5] J. Ambjorn and A. Ipsen, *Phys. Rev. D* **88**, 067502 (2013), [arXiv:1305.3148](https://arxiv.org/abs/1305.3148) [hep-th].
- [6] A. Candido, G. Clemente, M. D’Elia, and F. Rottoli, *JHEP* **04**, 184 (2021), [arXiv:2010.15714](https://arxiv.org/abs/2010.15714) [hep-lat].
- [7] G. Clemente and M. D’Elia, “Spectral Observables and Gauge Field Couplings in Causal Dynamical Triangulations,” in *Handbook of Quantum Gravity*, edited by C. Bambi, L. Modesto, and I. Shapiro (Springer Nature Singapore, Singapore, 2023) pp. 1–34.
- [8] M. Creutz, *Phys. Rev. D* **21**, 2308 (1980).
- [9] N. Cabibbo and E. Marinari, *Phys. Lett. B* **119**, 387 (1982).
- [10] B. Berg, *Phys. Lett. B* **104**, 475 (1981).
- [11] Y. Iwasaki and T. Yoshie, *Phys. Lett. B* **131**, 159 (1983).
- [12] S. Itoh, Y. Iwasaki, and T. Yoshie, *Phys. Lett. B* **147**, 141 (1984).
- [13] M. Teper, *Phys. Lett. B* **162**, 357 (1985).
- [14] E.-M. Ilgenfritz, M. L. Laursen, G. Schierholz, M. Muller-Preussker, and H. Schiller, *Nucl. Phys. B* **268**, 693 (1986).
- [15] M. Campostrini, A. Di Giacomo, H. Panagopoulos, and E. Vicari, *Nucl. Phys. B* **329**, 683 (1990).
- [16] B. Alles, L. Cosmai, M. D’Elia, and A. Papa, *Phys. Rev. D* **62**, 094507 (2000), [arXiv:hep-lat/0001027](https://arxiv.org/abs/hep-lat/0001027).
- [17] C. Bonati and M. D’Elia, *Phys. Rev. D* **89**, 105005 (2014), [arXiv:1401.2441](https://arxiv.org/abs/1401.2441) [hep-lat].
- [18] P. Scott Mara, *Journal of Combinatorial Theory, Series A* **20**, 170 (1976).
- [19] J. Ambjorn, Z. Drogosz, J. Gizbert-Studnicki, A. Görlich, J. Jurkiewicz, and D. Nemeth, *Phys. Rev. D* **94**, 044010 (2016), [arXiv:1604.08786](https://arxiv.org/abs/1604.08786) [hep-th].
- [20] L. Del Debbio, H. Panagopoulos, and E. Vicari, *JHEP* **08**, 044 (2002), [arXiv:hep-th/0204125](https://arxiv.org/abs/hep-th/0204125).
- [21] C. Bonati, M. D’Elia, and A. Scapellato, *Phys. Rev. D* **93**, 025028 (2016), [arXiv:1512.01544](https://arxiv.org/abs/1512.01544) [hep-lat].
- [22] E. Witten, *Nucl. Phys. B* **156**, 269 (1979).
- [23] G. Veneziano, *Nucl. Phys. B* **159**, 213 (1979).
- [24] J. Ambjorn, J. Gizbert-Studnicki, A. Görlich, J. Jurkiewicz, and D. Németh, *JHEP* **07**, 166 (2019), [arXiv:1906.04557](https://arxiv.org/abs/1906.04557) [hep-th].
- [25] J. Ambjorn, J. Gizbert-Studnicki, A. Görlich, J. Jurkiewicz, and D. Németh, *JHEP* **06**, 111 (2018), [arXiv:1802.10434](https://arxiv.org/abs/1802.10434) [hep-th].
- [26] J. Ambjorn, A. Gorlich, J. Jurkiewicz, R. Loll, J. Gizbert-Studnicki, and T. Trzesniewski, *Nucl. Phys. B* **849**, 144 (2011), [arXiv:1102.3929](https://arxiv.org/abs/1102.3929) [hep-th].
- [27] J. Ambjorn, A. Gorlich, J. Jurkiewicz, and R. Loll, *Phys. Rev. D* **78**, 063544 (2008), [arXiv:0807.4481](https://arxiv.org/abs/0807.4481) [hep-th].
- [28] G. ’t Hooft, *Phys. Rev. D* **14**, 3432 (1976).
- [29] J. Ambjorn, Z. Drogosz, J. Gizbert-Studnicki, A. Görlich, J. Jurkiewicz, and D. Németh, *Eur. Phys. J. C* **81**, 708 (2021), [arXiv:2101.08617](https://arxiv.org/abs/2101.08617) [gr-qc].
- [30] J. Ambjorn, Z. Drogosz, J. Gizbert-Studnicki, A. Görlich, J. Jurkiewicz, and D. Németh, *Phys. Rev. Lett.* **127**, 161301 (2021), [arXiv:2103.00198](https://arxiv.org/abs/2103.00198) [hep-th].
- [31] J. Ambjorn, Z. Drogosz, J. Gizbert-Studnicki, A. Görlich, J. Jurkiewicz, and D. a. Németh, *Class. Quant. Grav.* **38**, 195030 (2021), [arXiv:2105.10086](https://arxiv.org/abs/2105.10086) [gr-qc].